ChemComm

# Stable Melt Formation of 2D Nitrile-Based Coordination Polymer and Hierarchical Crystal–Glass Structuring



| | |
|---|---|
| Journal: | *ChemComm* |
| Manuscript ID | CC-COM-05-2020-003691.R1 |
| Article Type: | Communication |
| | |

COMMUNICATION

# Stable Melt Formation of 2D Nitrile-Based Coordination Polymer and Hierarchical Crystal–Glass Structuring

Chinmoy Das,[a] Tomohiro Ogawa[b] and Satoshi Horike*[a,b,c,d]

Received 00th January 20xx,
Accepted 00th January 20xx

DOI: 10.1039/x0xx00000x

**Crystal melting and vitrification of nitrile-based two-dimensional coordination polymer (CP) were studied. The crystal melts at 169 °C and has a wide liquid-state temperature window of over 110 °C. The crystalline state transformed to glassy state by melt-quench or mechanical milling. The mechanically induced glass showed permanent porosity, and it also showed glass-to-crystal transformation upon solvent treatment. Surface crystallization on top of grain-boundary-free glass monolith was demonstrated.**

In the last few years, crystal melting and the formation of glasses consisting of coordination polymers (CPs) and metal–organic frameworks (MOFs) have gained research interest.[1-4] The non-crystalline properties of these materials offer unique functions such as fast and selective gas/ion transport and hybridization with other substances for sensing and optical functions.[5, 6] Additionally, moldability and crystal-to-glass transformation are attractive for adhesive and switching materials.[7] However, the ligand system for constructing melting/vitrifying CP/MOFs remains limited. Most reported cases are metal–azolates (M = $Zn^{2+}$, $Co^{2+}$: ZIF-4, ZIF-62, etc.)[2, 8] and metal–azolate–phosphates (M = $Zn^{2+}$, $Cd^{2+}$, $Cr^{2+}$, $Mn^{2+}$).[1, 9-11] Substituent or mixing azolates are incorporated to modulate glass properties.[11-13] Recently, some of CPs made by thiocyanate and dicyanamide were also found to form glassy states.[14, 15] This includes our recent report on [Ag(*p*L2)($CF_3SO_3$)]·2$C_6H_6$ (*p*L2 = 1,3,5-tris(4-cyanophenylethynyl)benzene)) showing a narrow temperature window (10 °C) of liquid state.[16] All the examples of ZIFs have a melting temperature above 400 °C, and in many cases they have a narrow temperature window for the liquid state, which makes material handling difficult. Thus, it is important to develop a new family of melting/vitrifying structures to address these issues.

One useful ligand family with a tunable size and dimensionality is nitriles. Prussian blue analogues and Hofmann clathrates are inorganic nitrile (cyanide)-based CPs,[17, 18] and many crystal structures with organic nitrile ligands have been reported.[19, 20] In addition to designability, the coordination bond between the nitrile group and metal ions is labile and dynamic, which would contribute to crystal melting.[21] With this aim, we studied 2D [Ag(*m*L1)($CF_3SO_3$)]·2$C_6H_6$ (**1-a**, *m*L1 = 1,3,5-tris(3-cyanophenylethynyl)benzene), the crystal structure of which was reported in 1995.[22] In the original study, thermogravimetric analysis (TGA) suggested potential melting of the crystal. We investigated the crystal melting and glass formation characteristics by differential scanning calorimetry (DSC) and infrared spectroscopy (IR). The structure of the glassy state was characterized by X-ray absorption (XAS) and X-ray total scattering analysis. We confirmed a temperature window greater than 110 °C for the liquid state, which is one of the largest among reported CP/MOFs, as well as microporosity in the glassy state. Owing to its facile handling in air on a large scale, a grain-boundary-free glass monolith was fabricated. Moreover, we treated the glass monolith with benzene to induce surface crystallization with an adhesive crystal–glass interface.

The 2D CP was synthesized by a solvothermal reaction (Fig. 1).[22] An asymmetric unit consists of one $Ag^+$, one *m*L1, and one $CF_3SO_3^-$, as well as two benzene solvent molecules. The four coordination sites of each $Ag^+$ are satisfied by three –C≡N groups from three different *m*L1 and one $CF_3SO_3^-$, creating a distorted trigonal pyramidal geometry. The bridging of *m*L1 to each $Ag^+$ forms an extended 2D layered structure. Each layer is stacked in an ···ABCD··· fashion, creating channels filled with guest benzene molecules. We confirmed that the powder X-ray diffraction (PXRD) pattern of **1-a** is identical to the simulated pattern from the proposed crystal structure (Fig. 1). TGA of **1-a**

[a] *AIST-Kyoto University Chemical Energy Materials Open Innovation Laboratory (ChEM-OIL), National Institute of Advanced Industrial Science and Technology (AIST), Yoshida-Honmachi, Sakyo-ku, Kyoto 606-8501, Japan*
[b] *Institute for Integrated Cell-Material Sciences, Institute for Advanced Study, Kyoto University, Yoshida-Honmachi, Sakyo-ku, Kyoto 606-8501, Japan*
[c] *Department of Synthetic Chemistry and Biological Chemistry, Graduate School of Engineering, Kyoto University, Katsura, Nishikyo-ku, Kyoto 615-8510, Japan*
[d] *Department of Materials Science and Engineering, School of Molecular Science and Engineering, Vidyasirimedhi Institute of Science and Technology, Rayong 21210, Thailand*

†Electronic Supplementary Information (ESI) available: Experimental details, PXRD, FT-IR, XAS, PDF and adsorption isotherms. See DOI: 10.1039/x0xx00000x

showed a stepwise weight loss from 25 to 145 °C corresponding to the release of guest benzene molecules (16 wt%, Fig. S1).

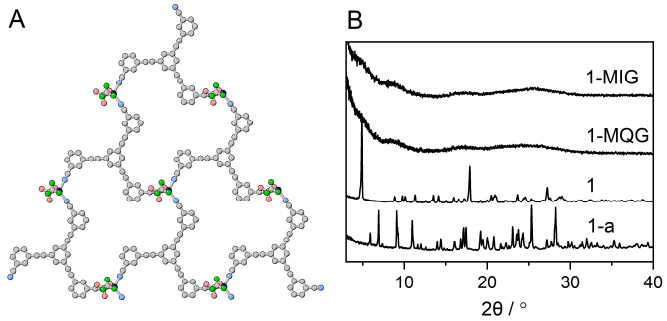


**Fig. 1** (A) Crystal structure of layer [Ag(*m*L1)($CF_3SO_3$)]·2$C_6H_6$ (**1-a**). Gray: C, Purple: N, Pink: O, Yellow: S, Green: F, Black: Ag. Hydrogen and guest benzene molecules are omitted. (B) PXRD patterns of **1-a**, **1**, **1-MQG** (melt quenched glass) and **1-MIG** (mechanically induced glass) measured at room temperature.

According to the TGA observations, we degassed **1-a** under vacuum at 140 °C for 6 h to obtain **1**, which showed a different PXRD pattern than that of **1-a**, meaning that the structure changed upon desolvation (Fig. 1). Although we have not succeeded in solving the crystal structure of **1** because of the loss of single crystallinity, we investigated its structure by XAS, FT-IR, PXRD, and elemental analysis. XAS measurements were performed for **1-a** and **1** to understand the local structural arrangements around $Ag^+$. The Ag *K*-edge X-ray absorption near edge structure (XANES) region of **1** showed a similar energy and shape to **1-a** (Fig. S2), suggesting that Ag maintains its +1 oxidation state by the core–shell 1s to 5p electronic transition at 25516 eV in both **1-a** and **1**. The Fourier-transformed Ag *K*-edge extended X-ray absorption fine structure (EXAFS) spectra confirmed that scattering pathways for the two main components appeared in the radial distribution functions (RDFs) located at 1.2–2.0 and 2.1–3.2 Å (Fig. S2). The scattering pathways of Ag-O/Ag-N and other neighboring atoms fall in similar RDFs for both **1-a** and **1**. We attempted to fit the $K^3$-weighted RDFs of **1-a** and **1** using IFEFFIT calculations (See ESI). The obtained set of converged parameters suggested that the coordination number around $Ag^+$ is (4.3 ± 0.9) and (4.1 ± 1.4) for **1-a** and **1**, respectively (Fig. S3 and Table S1).

FT-IR confirmed a strong −C≡N stretching vibration band at 2254 $cm^{-1}$ for **1-a** from the *m*L1 bridges to $Ag^+$. The −C≡N stretching vibration of *m*L1 alone appears at 2230 $cm^{-1}$, which confirms that the bridging of *m*L1 to $Ag^+$ causes a 24 $cm^{-1}$ shift to a higher frequency (Fig. S4).[23] FT-IR also confirmed that two different −C≡N stretching peaks appeared at 2255 and 2232 $cm^{-1}$ in the spectrum of the distorted structure of **1**. The coupling of stretching motions between nitrile bonds often results in such splitting of the nitrile vibration band.[24, 25] With these XAS and FT-IR results, we concluded that **1** retains an extended network structure consisting of $Ag^+$ and *m*L1 to form a CP with the same coordination environment around $Ag^+$. TGA of **1** showed no weight loss up to 280 °C (Fig. S1). DSC measurement of **1** at 10 °C $min^{-1}$ with *in situ* image collection showed an endothermic peak at 169 °C (Fig. 2), indicating crystal melting. Considering no weight loss was observed for **1** below 280 °C by TGA, the temperature window of the liquid state of **1** is greater than 110 °C. This is one of the widest temperature windows among other reported liquid states of CP/MOFs.[4] On a similar note, the liquid state of [$Zn(Im)_{1.33}$(5-mbIm)$_{0.67}$] (ZIF-76-mbIm) was found to be stable over a temperature range of 120 °C.[26]

We observed a glass transition ($T_g$) at 68 °C during the DSC cooling process, below which we obtained the glassy state of **1** (Fig. 2). We denote this melt-quenched glass as **1-MQG**. In the second DSC heating cycle, we again found $T_g$ at 68 °C and no crystallization up to 200 °C. The DSC profiles remained unchanged for six cycles of heating and cooling (Fig. S5). FT-IR of **1-MQG** showed −C≡N vibration bands at 2252 and 2232 $cm^{-1}$ (Fig. S4). The amorphous behavior of **1-MQG** was characterized by PXRD as shown in Fig. 1. TGA of **1-MQG** suggested that no weight loss occurred up to 280 °C, and the glassy state showed a high thermal stability without crystallization or degradation (Fig. S5-S6).

Vitrification led by hand-grinding method was previously reported.[16] We conducted hand-grinding of microcrystals of **1** with an agate mortar under an Ar atmosphere for 30 min to obtain homogeneous glass sample. **1** was thus transformed into **1-MIG** (mechanically induced glass), the amorphous structure of which was confirmed by PXRD (Fig. 1). DSC of **1-MIG** determined that the glass transition temperature ($T_g$ = 68 °C) was identical to that of **1-MQG**. In contrast, **1-MIG** crystallized at $T_c$ = 102 °C (Fig. 2B), which we did not observe for **1-MQG**. We performed hand-grinding of **1-MQG** monolith in agate mortar under Ar for 2 min. We observed $T_c$ at 130 °C for the powdered **1-MQG**, this behavior was similar with **1-MIG** (Fig. S7). Downsizing of the particle of **1-MQG** increases the surface area, and it leads higher probability of crystal nucleation for crystallization. We heated **1-MIG** at 120 °C for 1 h, and the resultant sample showed the same PXRD pattern as that of **1** (Fig. S8). The enthalpy of crystallization ($\Delta H_c$) for **1-MIG** was −32 J $g^{-1}$, which is comparable to that of some representative organic polymers such as polylactic acid and metallic glasses ($Pd_{39}Ni_{10}Cu_{30}P_{21}$).[27, 28] Further DSC heating resulted in a single melting peak ($T_m$) at 168 °C, which is the same as that of pristine **1**. In the second DSC heating cycle, $T_g$ was observed at 68 °C, and no $T_m$ was observed up to 180 °C. $T_g$ was also observed at 68 °C during the second cooling process.

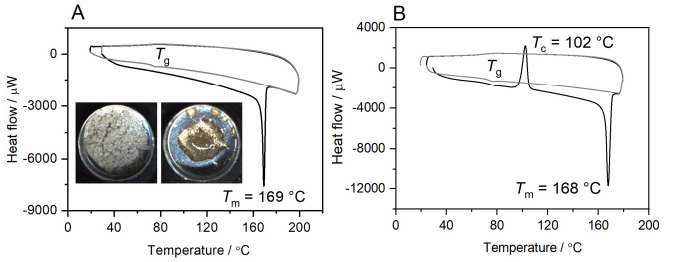


**Fig. 2** Two cycles of heating and cooling processes (1st: black, 2nd: gray) of DSC profiles of (A) **1** and (B) **1-MIG**. *In situ* snapshots of **1** at 25 and 169 °C in the first heating process are also shown. $T_g$, $T_m$ and $T_c$ represent the glass transition, crystallization and melting temperatures, and the ramping rate is 10 °C $min^{-1}$.

FT-IR of **1-MIG** showed the −C≡N vibration bands at 2253 and 2233 $cm^{-1}$, the same as those of **1** and **1-MQG** (Fig. S4). Ag *K*-edge XANES and EXAFS suggest that **1-MIG** maintains its +1 oxidation state (Fig. S2), and scattering pathways fall under similar RDFs to those of **1-a** and **1** (Fig. S2). We fitted the $K^3$-weighted RDF of **1-MIG** and fitted coordination number around $Ag^+$ is (4.1 ± 1.2) showed that **1-MIG** maintained a similar geometry to that of **1-a** and **1** (Fig. S3 and Table S1). X-ray total scattering structure functions (*S*(Q)) and corresponding reduced pair distribution functions (*G*(r)) were studied (Fig. S9), which showed correlations above 7 Å in **1-MIG** due to the contribution of *m*L1. The intense peak at 2.2–2.4 Å involves the radial distribution of Ag-O and Ag-N coordination bonds.

To investigate the permanent porosity of the samples,[11, 26] we performed $CO_2$ gas adsorption studies at −78.15 °C for **1**, **1-MQG**, and **1-MIG** (Fig. S10). Although **1** and **1-MQG** showed negligible uptakes, **1-MIG** showed a gradual uptake from the low-pressure regime, reaching 18 mL $g^{-1}$ at 102 kPa. The desorption isotherm did not show a hysteresis, and PXRD suggests **1-MIG** remained amorphous after the $CO_2$ adsorption experiment. Although the uptake amount was not high, we confirmed the microporosity of **1-MIG**. On the other hand, we observed the glass-to-crystal transformation from **1-MIG** to **1-a** upon exposure to benzene vapor at 25 °C and confirmed by PXRD (Fig. 3). **1-MIG** showed a two-stepwise adsorption isotherm of benzene vapor at 25 °C (Fig. 3A). The gate-opening pressures for adsorption were 2.3 and 6.2 kPa, and the total uptake was 64.1 mL $g^{-1}$ at $P_e$ = 12.3 kPa. A stepwise adsorption isotherm represents structural transformation[29] and herein the steps are attributed to crystallization. To investigate this structural transformation, we measured the PXRD patterns (Fig. 3B) of samples adsorbing different amounts of benzene vapor. For this analysis, we retrieved two states of **1-MIG** during benzene adsorption at 2.8 and 12.3 kPa (points (i) and (ii) in Fig. 3A, respectively). Note that the uptake amounts of benzene for each pressure point remained unchanged during the PXRD studies as confirmed by TGA. At pressure point (i), the crystallization had already started. The PXRD pattern at point (ii) was almost identical to that of **1-a** except for a single peak at 2θ of 5.4°, and the pattern at point (iii) was identical to that of **1-a**. The broad hysteresis in the sorption profile suggests that the interaction of the framework and benzene solvent is strong in **1-MIG**, which enhances the crystallization.

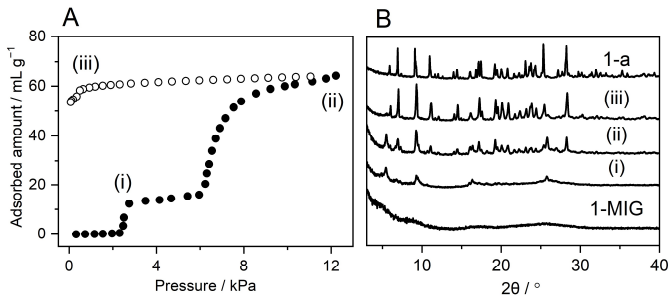


**Fig. 3** (A) Sorption isotherms of benzene vapour on **1-MIG** at 25 °C. Solid and open circles represent adsorption and desorption. (B) PXRD patterns of **1-MIG** at different vapour pressures points shown in Fig. 3A. PXRD pattern of pristine **1-a** is also shown for comparison.

One of the advantages of glass is its soft mechanical properties. Subsequently, we fabricated a monolith of **1-MIG** through the hot-press technique (See ESI). The process provided a monolith, which we denote as **1-MIG-m**. PXRD analysis of **1-MIG-m** showed no Bragg diffraction, suggesting the glassy nature was intact (Fig. S11), and the TGA profile showed no weight loss up to 280 °C. The DSC profile of **1-MIG-m** acquired at 10 °C $min^{-1}$ exhibited a glass transition at $T_g$ = 71 °C and subsequent crystallization at $T_c$ = 110 °C (Fig. S11). Further heating resulted in melting with an endothermic peak at 166 °C, and it showed the same thermal behavior as **1-MIG**.

We performed benzene adsorption studies of **1-MIG-m** at 25 °C (Fig. S12). We found the total uptake was 27 mL $g^{-1}$ at $P_e$ = 12.3 kPa, which is approximately half of that of **1-MIG**. The decreased uptake and shift in the gate-opening pressure for **1-MIG-m** are attributable to the slower vapor/gas diffusion kinetics in the monolith. PXRD analysis suggested that partial glass-to-crystal transformation occurred in **1-MIG-m** (Fig. S12). Since we found that the crystallization of **1-MIG-m** was induced by benzene, we tried to observe crystallization on the monolith surface. The controlled crystallization of specific domains in glasses has been shown to be important for preparing glass–ceramic materials,[30] but it has not been attempted for any CP/MOFs.

We soaked a 2 mm diameter and 0.3 mm thickness **1-MIG-m** in anhydrous benzene and collected cross-sectional SEM images after different soaking periods (Fig. 4). The pristine **1-MIG-m** has no inner and surface grain boundaries (Fig. 4A). The cross-sectional SEM image of the sample suggests that the crystallization from the surface propagated upon continued benzene soaking (Fig. 4B). Linear cracks perpendicular to the layer arising from the volume change induced by crystallization (Fig. 4C). The interface between the crystalline and glass domains was smooth and in good contact.

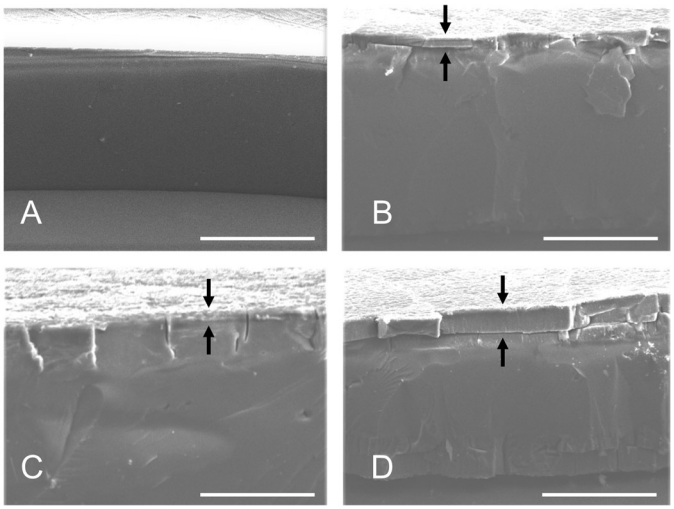


**Fig. 4** (A) Cross-section SEM image of pristine **1-MIG-m**. (B-D) The time-course SEM cross-section images of **1-MIG-m** after soaking in anhydrous benzene for 4 h, 16 h and 24 h at 25 °C, respectively. Scale bars are 100 μm and the width of crystallized surface are highlighted in arrows.

Further soaking (24 h, Fig. 4D) generated a distinct crystalline layer with a thickness of ca. 20 μm with an interfacial boundary

between the crystal and glass. This approach of surface crystallization of glass would be useful for membrane applications. Additionally, hand-grinding of **1-a** under Ar also formed glassy state confirmed by PXRD and DSC (Fig. S13). The prepared glass accommodates benzene as a guest.

In conclusion, a new family of CP/MOF glasses, we fabricated $[Ag(m\text{L1})(CF_3SO_3)]\cdot 2C_6H_6$ composed of $Ag^+$ and a planar tripodal nitrile ligand. The guest-free structure underwent crystal melting at 169 °C. The temperature window of its liquid state is over 110 °C, which is one of the largest among known melting CP/MOFs. Glassy states were fabricated by either melt-quenching or mechanical milling of the polycrystalline sample. The mechanically induced glass maintained the same coordination environment around $Ag^+$ as the crystalline state as determined by X-ray absorption, X-ray total scattering, and FT-IR studies. $CO_2$ gas sorption analysis of the mechanically induced glass indicated its permanent porosity. We made a grain-boundary-free glass monolith by a facile hot-press process and demonstrated its surface crystallization by solvent treatment. By the use of solvent-induced crystallization, we observed 20 μm thick uniform crystalline layer on top of grain-boundary-free glass. This work clarified that nitriles are a promising new ligand family for CP/MOF liquids and glasses because of their wide liquid-state temperature window, microporosity, and controllable crystallization in their glass structures.

The work was supported by the Japan Society of the Promotion of Science (JSPS) for a Grant-in-Aid for Scientific Research (B) (JP18H02032), Challenging Research (Exploratory) (JP19K22200) from the Ministry of Education, Culture, Sports, Science and Technology, Japan, and Strategic International Collaborative Research Program (SICORP), Adaptable and Seamless Technology Transfer Program through Target-driven R&D (A-STEP) from the Japan Science and Technology, Japan. We acknowledge Aichi Synchrotron Radiation Center BL11S2 beamline for XAS and SPring-8 BL04B2 beamline for PXRD.

## Conflicts of interest

There are no conflicts to declare.

## References

1. D. Umeyama, S. Horike, M. Inukai, T. Itakura and S. Kitagawa, *J. Am. Chem. Soc.*, 2015, **137**, 864-870.
2. T. D. Bennett, J. C. Tan, Y. Yue, E. Baxter, C. Ducati, N. J. Terrill, H. H. Yeung, Z. Zhou, W. Chen, S. Henke, A. K. Cheetham and G. N. Greaves, *Nat. Commun.*, 2015, **6**, 8079.
3. T. D. Bennett and S. Horike, *Nat. Rev. Mater.*, 2018, **3**, 431-440.
4. S. Horike, S. S. Nagarkar, T. Ogawa and S. Kitagawa, *Angew. Chem., Int. Ed.*, 2020, **59**, 2-15.
5. W. Chen, S. Horike, D. Umeyama, N. Ogiwara, T. Itakura, C. Tassel, Y. Goto, H. Kageyama and S. Kitagawa, *Angew. Chem. Int. Ed.*, 2016, **55**, 5195-5200.
6. A. Qiao, H. Tao, M. P. Carson, S. W. Aldrich, L. M. Thirion, T. D. Bennett, J. C. Mauro and Y. Yue, *Opt. Lett.*, 2019, **44**, 1623-1625.
7. S. S. Nagarkar, S. Horike, T. Itakura, B. Le Ouay, A. Demessence, M. Tsujimoto and S. Kitagawa, *Angew. Chem. Int. Ed.*, 2017, **56**, 4976-4981.
8. T. D. Bennett, Y. Yue, P. Li, A. Qiao, H. Tao, N. G. Greaves, T. Richards, G. I. Lampronti, S. A. Redfern, F. Blanc, O. K. Farha, J. T. Hupp, A. K. Cheetham and D. A. Keen, *J. Am. Chem. Soc.*, 2016, **138**, 3484-3492.
9. S. Horike, D. Umeyama, M. Inukai, T. Itakura and S. Kitagawa, *J. Am. Chem. Soc.*, 2012, **134**, 7612-7615.
10. Y. Ohara, A. Hinokimoto, W. Chen, T. Kitao, Y. Nishiyama, Y. L. Hong, S. Kitagawa and S. Horike, *Chem. Commun.*, 2018, **54**, 6859-6862.
11. M. Inukai, Y. Nishiyama, K. Honjo, C. Das, S. Kitagawa and S. Horike, *Chem. Commun.*, 2019, **55**, 8528-8531.
12. L. Frentzel-Beyme, M. Kloss, P. Kolodzeiski, R. Pallach and S. Henke, *J. Am. Chem. Soc.*, 2019, **141**, 12362-12371.
13. J. Hou, L. Rios, A. Krajnc, A. McCaul, S. Li, A. Bumstead, A. Sapnik, Z. Deng, R. Lin, P. A. Chater, D. S. Keeble, D. A. Keen, D. Appadoo, B. Chan, V. Chen, G. Mali and T. D. Bennett, *J. Am. Chem. Soc.*, 2020, **142**, 3880-3890.
14. S. S. Nagarkar, H. Kurasho, N. T. Duong, Y. Nishiyama, S. Kitagawa and S. Horike, *Chem. Commun.*, 2019, **55**, 5455-5458.
15. B. K. Shaw, A. R. Hughes, M. Ducamp, D. A. Keen, F.-X. Coudert, F. Blanc and T. D. Bennett, *ChemRxiv*, 2020, DOI: 10.26434/chemrxiv.11956599.v1.
16. C. Das and S. Horike, *Faraday Discuss.*, 2020, DOI: 10.1039/D0FD00003E.
17. K. A. Hofmann and F. Küspert, *Z. Anorg. Allg. Chem.*, 1897, **15**, 204-207.
18. J. F. Keggin and F. D. Miles, *Nature*, 1936, **137**, 577-578.
19. Y. Kinoshita, I. Matsubara, T. Higuchi and Y. Saito, *Bull. Chem. Soc. Jpn.*, 1959, **32**, 1221-1226.
20. B. F. Hoskins and R. Robson, *J. Am. Chem. Soc.*, 1989, **111**, 5962-5964.
21. D. Venkataraman, S. Lee, J. S. Moore, P. Zhang, K. A. Hirsch, G. B. Gardner, A. C. Covey and C. L. Prentice, *Chem. Mater.*, 1996, **8**.
22. D. Venkataraman, G. B. Gardner, S. Lee and J. S. Moore, *J. Am. Chem. Soc.*, 1995, **117**, 11600-11601.
23. T. Ueda, T. Tominaga, T. Mochida, K. Takahashi and S. Kimura, *Chem. Eur. J.*, 2018, **24**, 9490-9493.
24. E. V. Dikarev, B. Li, V. V. Chernyshev, R. V. Shpanchenko and M. A. Petrukhina, *Chem. Commun.*, 2005, 3274-3276.
25. A. A. Schilt, *Inorg. Chem.*, 1964, **3**, 1323-1325.
26. C. Zhou, L. Longley, A. Krajnc, G. J. Smales, A. Qiao, I. Erucar, C. M. Doherty, A. W. Thornton, A. J. Hill, C. W. Ashling, O. T. Qazvini, S. J. Lee, P. A. Chater, N. J. Terrill, A. J. Smith, Y. Yue, G. Mali, D. A. Keen, S. G. Telfer and T. D. Bennett, *Nat. Commun.*, 2018, **9**, 5042.
27. E. A. R. Duek, C. A. C. Zavaglia and W. D. Belangero, *Polymer*, 1999, **40**, 6465-6473.
28. L.-M. Wang, G. Li, Z. J. Zhan, L. L. Sun and W. K. Wang, *Philos. Mag. Lett.*, 2001, **81**, 419-423.
29. G. Férey and C. Serre, *Chem. Soc. Rev.*, 2009, **38**, 1380-1399.
30. W. Wisniewski, K. Takano, Y. Takahashi, T. Fujiwara and C. Rüssel, *Sci. Rep.*, 2015, **5**, 9069.

2D nitrile-based coordination polymer crystal shows over 110 °C of windows of liquid state and it forms glass monolith.

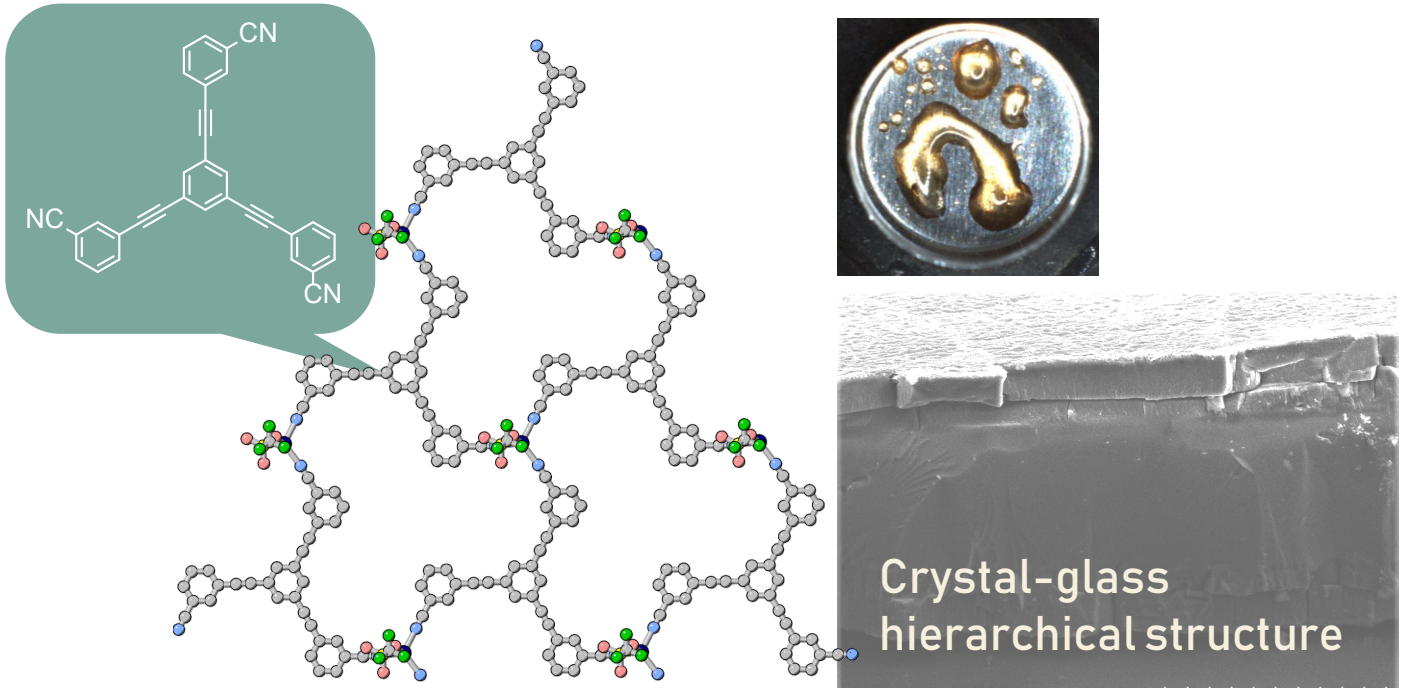
CN
NC
CN
Crystal-glass
hierarchical structure